Molecular Therapy
Nucleic Acids
Original Article

Peptide nanostructures-based delivery of DNA nanomaterial therapeutics for regulating gene expression

Bineeth Baral,[1,2,7] Bijayananda Panigrahi,[3,4,7] Avishek Kar,[1,2] Kiran D. Tulsiyan,[5,6] Uday Suryakant,[3] Dindyal Mandal,[3] and Umakanta Subudhi[1,2]

[1]DNA Nanotechnology & Application Laboratory, Environment & Sustainability Department, CSIR-Institute of Minerals & Materials Technology, Bhubaneswar 751013, Odisha, India; [2]Academy of Scientific & Innovative Research (AcSIR), Ghaziabad 201002, India; [3]School of Biotechnology, Kalinga Institute of Industrial Technology Deemed to be University, Bhubaneswar 751024, Odisha, India; [4]Biopioneer Private Limited, Bhubaneswar 751024, Odisha, India; [5]School of Chemical Sciences, National Institute of Science Education & Research, Bhubaneswar 752050, India; [6]Homi Bhaba National Institute, Mumbai 400094, India

Self-assembled branched DNA (bDNA) nanomaterials have exhibited their functionality in various biomedical and diagnostic applications. However, the anionic cellular membrane has restricted the movement of bDNA nanostructures. Recently, amphiphilic peptides have been investigated as cationic delivery agents for nucleic acids. Herein, we demonstrate a strategy for delivering functional bDNA nanomaterials into mammalian cells using self-assembled linear peptides. In this study, antisense oligonucleotides of vascular endothelial growth factor (VEGF) were inserted in the overhangs of bDNAs. Novel linear peptides have been synthesized and the peptide-bound bDNA complex formation was examined using various biophysical experiments. Interestingly, the W4R4-bound bDNAs were found to be exceptionally stable against DNase I compared to other complexes. The delivery of fluorescent-labeled bDNAs into the mammalian cells confirmed the potential of peptide transporters. Furthermore, the functional efficacy of the peptide-bound bDNAs has been examined through RT-PCR and western blot analysis. The observed results revealed that W4R4 peptides exhibited excellent internalization of antisense bDNAs and significantly suppressed (3- to 4-fold) the transcripts and translated product of VEGF compared to the control. In summary, the results highlight the potential use of peptide-based nanocarrier for delivering bDNA nanostructures to regulate the gene expression in cell lines.

INTRODUCTION

Nucleic acid-based therapy has gained attention due to their high specificity, efficiency, and easy of synthesis.[1] However, therapeutics such as small interfering RNA (siRNAs), anti-microRNAs (anti-miRNAs), or antisense oligonucleotides containing 21 to 27 bp sequences are less stable with high thermal sensitivity leading to degradation during the process of delivery.[2,3] Recently, the self-assembled branched DNA (bDNA) nanostructures have been explored as a novel therapeutic agent because of several unique features, such as simpler self-assembly process, defined geometry, programmable complementarity, versatile designing, thermostability, affordable synthesis, and ease of modifications.[4,5] These designed therapeutic DNA nanomaterials can carry anticancer drugs, antisense oligonucleotides (ASOs), photosensitizers, nanoparticles, and proteins.[6–9] However, bDNA nanostructures have been held up due to weak targeting of specific cells, poor bioavailability, and meager cellular uptake.[10] The delivery of bDNA is challenging because of the large negatively charged phosphate backbone and high molecular mass compared to siRNAs, which prevent cellular permeability.[11] Therefore, a suitable carrier with a positive charge is needed for the delivery of bDNA nanostructures. Nevertheless, highly positive polymeric nanoparticles could lead to cytotoxicity and cellular apoptosis.[12–14] Hence, self-assembled peptide nanocarriers having less positive charge could be useful to overcome this issue.

Over the last decade, several cationic polymers, cell-penetrating peptides, nanoparticles, and liposomes were designed as vectors to transfect nucleic acids to mammalian cells; among the vectors, peptides and peptide-based self-assembled nanostructures have drawn much attention from peptide chemists and biologists because of their chemical and physical stability.[15–18] Simple structure and shape of peptides with easy synthesis in bulk amounts are possible by varying amino acid residues with different functional groups of a hydrophobic and hydrophilic nature. Very few peptide-based carriers, such as MPG, Xentry-KALA (XK), Xentry-Protamine (XP), TAT, H5WYG

Received 13 January 2023; accepted 14 July 2023;
https://doi.org/10.1016/j.omtn.2023.07.017.

[7]These authors contributed equally

Correspondence: Dr Dindyal Mandal, School of Biotechnology, Kalinga Institute of Industrial Technology Deemed to Be University, Bhubaneswar 751024, Odisha, India.
E-mail: dmandal@kiitbiotech.ac.in
Correspondence: Dr Umakanta Subudhi, DNA Nanotechnology & Application Laboratory, Environment & Sustainability Department, CSIR-Institute of Minerals & Materials Technology, Bhubaneswar 751013, Odisha, India.
E-mail: usubudhi@immt.res.in

(GLFHAIAHFIHGGWHGLIHGWYG), and CPS 2, have been reported for the delivery of oligonucleotides.[19–24] Further, some of the peptides containing Trp and His or Arg residues, such as cyclo-[WH]5, linear [WH]5, and cyclo-[WR]5 were reported as small molecule transporters with less toxicity. In addition, cyclo-[WR]5, and its modified sequences CP I and CP III were reported as vehicles for siRNA delivery.[25–27] With this background, we aimed to design linear peptides that selectively bind bDNA and efficiently deliver bDNA-carrying nucleic acid therapeutics. In this regard, a series of linear peptides, including W4R4 (Ac-WWWWGGRRRR-Am), W3R3 (Ac-WWWGGGRRR-Am), W2R4 (Ac-WWGGGRRRR-Am), and W1R4 (Ac-WGGGRRRR-Am), have been designed and synthesized containing Trp and Arg residues. Similarly, the other class of peptides containing Trp and His amino acids are W4H4 (Ac-WWWWGG HHHH-Am), W3H4 (Ac-WWWGGHHHH-Am), W2H4 (Ac-WW GGGHHHH-Am), and W1H4 (Ac-WGGHHHH-Am). Thus, a class of self-assembled peptides was explored to carry bDNAs with ASOs for gene expression study. For the first time, we have demonstrated that these linear peptides are binding to bDNAs and successfully transfecting bDNA to cell lines. Biophysical interactions and thermodynamics have been thoroughly studied, and the transfecting ability of linear peptides was compared with the conventional transfecting agent Lipofectamine 2000. In a case study, the gene-silencing activity by peptide-mediated delivery of bDNA was also observed for vascular endothelial growth factor (VEGF), which accelerates tumor angiogenesis and metastasis.

The powerful angiogenic factor VEGF was initially identified as crucial for the proliferation of vascular endothelial cells. VEGF and the receptor of VEGF are highly expressed in many tumors and play an important role in tumor angiogenesis.[28] Nevertheless, the signaling protein VEGF promotes the growth of new blood vessels.[28–30] VEGF restores the blood supply to cells and tissues when they are deprived of oxygenated blood due to compromised blood circulation.[31,32] Since VEGF plays a major role in cancer proliferation, bDNA containing ASOs of VEGF was explored to downregulate VEGF expression using linear peptides as delivery agents.

RESULTS

Synthesis and characterization of self-assembled linear peptide nanostructures

The WR class of peptides include W4R4 (Ac-WWWWGGRRRR-Am), W3R3 (Ac-WWWGGGRRR-Am), W2R4 (Ac-WWGGGRR RR-Am), and W1R4 (Ac-WGGGRRRR-Am), whereas the WH set contains W4H4 (Ac-WWWWGGHHHH-Am), W3H4 (Ac-WWW GGHHHH-Am), W2H4 (Ac-WWGGGHHHH-Am), and W1H4 (Ac-WGGHHHH-Am), which are given in Table S1. Peptides were synthesized using solid-phase synthesis techniques (Figure S1) and purified through preparative high-pressure liquid chromatography (HPLC). Further, the molecular mass of the linear peptides was identified by mass spectrometry analysis (Table S2; Figures S2–S9).

WR and WH peptides were dissolved in water at a concentration of 2 mM, and the structural morphology was observed under high-resolution transmission electron microscopy (HR-TEM). All the linear peptides exhibited self-assembled micellar structures in an aqueous solution (Figure 1). The overall size was observed to be within 50 nm, whereas W4R4 and W4H4 formed high-density nanostructures (Figures 1D and 1H). Circular dichroism (CD) spectroscopy was used to examine the secondary conformations of linear peptides. The first two peptides (W1R4 and W1H4) feature a random turn-like topology that contains a short positive peak at 225 nm and a negative shoulder peak at 200 nm (Figures 2A and 2B). On the contrary, the resultant spectra of linear peptides having nine or 10 amino acids consequently have a positive shoulder peak at $\sim$ 210 nm and a dominantly negative peak at 225 nm due to the presence of an indole ring in the tryptophan group (Figures 2A and 2B). The peak was gradually distinct with increase in the length of peptides. Due to the distinct functional groups in the linear peptides, the R_h values of the WR and WH series ranged from 28 to 48 nm (Figures S10A and S10B; Table S1). The zeta potential of the linear peptides were found to be in the range of +5 to +20 mV, indicating sufficient positive charge (Figures S10C and S10D).

Characterization of self-assembled bDNA nanomaterials

bDNA monomers were derived from four single-stranded oligonucleotides that were reported earlier for self-assembly studies.[33–36] The oligonucleotides A and D were designed to carry two overhangs comprising scramble or ASOs of VEGF sequences (Table S3).[24] Likewise, the terminal segments of strands B and C had complementarity sequences to facilitate the process of self-assembly. The 30-nucleotide central region of strands A and D exhibited hybridization with strands B and C, respectively. In this study, bDNAaso was successfully developed for selective binding to VEGF mRNAs. The control bDNAscr contains scramble sequences in the overhang and is employed in all investigations to eliminate the potential confounding effects arising from the bDNA structures. The conformation of self-assembled products and their physiological stability have been demonstrated in agarose gel electrophoresis (AGE). Different combinations of single, di-, tri-, and tetra-oligonucleotides in equimolar ratios were allowed to self-assemble and then characterized for their differential migration in AGE (Figures 2C and 2D). Further, the biophysical interactions and binding kinetics were studied between bDNA and linear peptides.

Biophysical binding and thermodynamics of bDNAs with linear peptides

A gel retardation experiment was carried out to assess the binding affinities between bDNAaso nanostructures and linear peptides (W4R4 and W4H4) at various w/w ratios (10, 25, 50, 75, and 100). In the presence of W4H4 peptides, a sharp and clear band was observed for the bDNAaso, while the intensity gradually disappeared with the increasing ratio of W4R4 peptides, indicating a higher binding affinity of bDNA with W4R4 (Figures 2E and 2F). Interestingly, sharp and distinct bands were noticed in control bDNAs that were incubated without linear peptides and in the presence of His-rich linear peptides (Figures 2G and 2H). Intriguingly, the bDNA bands disappeared in the gel when Arg-rich linear peptides were incubated. Similarly, Alexa 488-bound

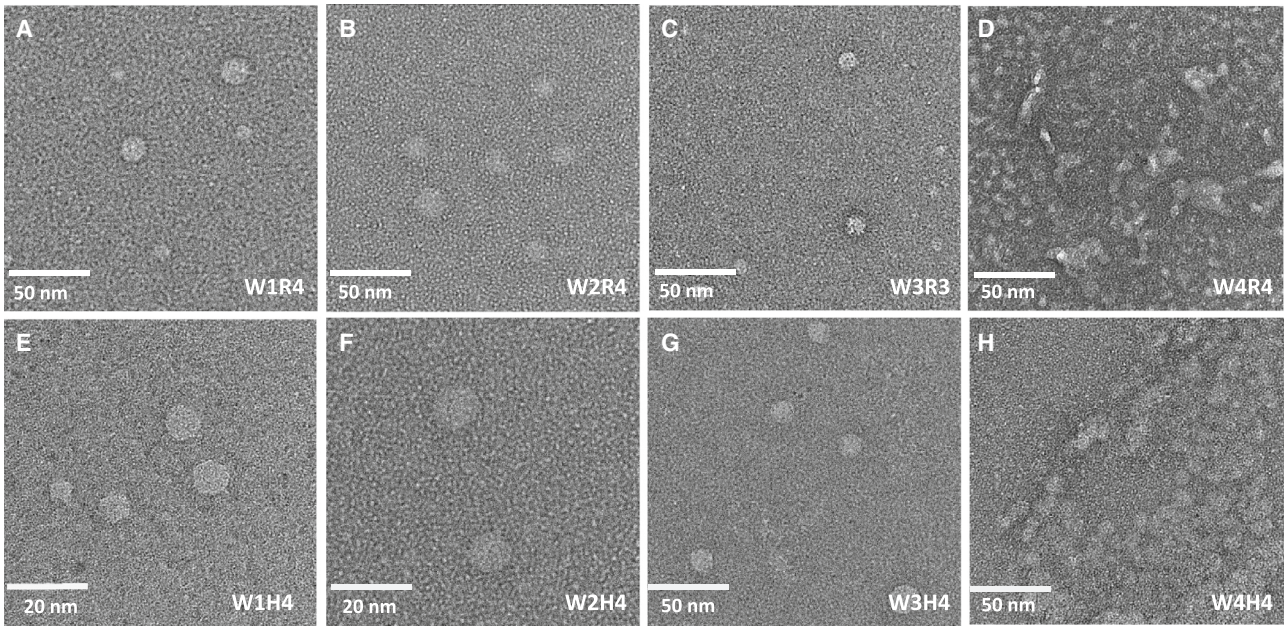

Figure 1. Characterization of the self-assembled linear peptides

HR-TEM images of self-assembled linear peptides. The top panel represents the WR series W1R4 (A), W2R4 (B), W3R3 (C), W4R4 (D), and the bottom panel represents the WH sets W1H4 (E), W2H4 (F), W3H4 (G), and W4H4 (H). All the linear peptides exhibited micellar structures in an aqueous solution within an overall size of 50 nm.

bDNAs were incubated with increasing concentrations of W4R4 and W4H4 peptides and analyzed in gel electrophoresis (Figures S11A and S11B). Interestingly, a similar binding pattern was observed for bDNAs in the presence of Alexa 488. Further, the absorbance studies were used to confirm the interaction between the linear peptides and Alexa 488 bDNAs.[37] With increasing molar ratios of W4R4 peptides, a significant decline in absorbance of DNA was observed, whereas no significant alteration in absorbance was noticed with W4H4 peptides. Thus, the hypochromic effect of Alexa 488 peak at 495 nm indicated W4R4 peptide-bDNA interaction (Figure S11). However, WR peptides bind more strongly to bDNAaso than bDNAscr. We cannot explain the reason at present. Further, the isothermal titration calorimetry (ITC) studies were carried out to understand the thermodynamics of interaction between bDNAs and linear peptides.

The top panel of the graph exhibits peptide interactions with bDNA, whereas the bottom panel depicts the heat released as a function of the biophysical interaction (Figure 3). Although the binding affinities of linear peptides to bDNAaso are identical to those of bDNAscr, the binding affinity of bDNAaso with W4R4 is about nine times higher than other peptide-bound bDNAs (Figure S12). This interaction prompted us to investigate the secondary conformational changes of bDNAs in the presence of linear peptides.

The characteristic CD spectra of B-form of bDNAaso at 245 and 278 nm were found to be decreased upon the increased concentration of linear peptides from 5 to 100 μM (Figure 4). Similar outcomes were observed for the WR and WH peptides toward the interaction with bDNAscr (Figure S13). Interestingly, the WR series show better binding to bDNA than the WH series. In the case of W4R4 peptide-bDNA complexes, the peak intensities of bDNA flattened to the baseline, indicating condensed and compact DNA (Figures 4G and S13G). The greater affinity of Arg-rich peptides toward bDNA compared to His-rich peptides motivated us to understand the surface interaction between the peptides and bDNAs.

Particle size and surface charge of peptide-bDNA complex

The R_h value of bDNAscr and bDNAaso was found to be 14 and 25 nm, respectively (Figures 5A and 5B). In the presence of bDNAs, a moderate increase in hydrodynamic radii was noticed for W3R3 and W3H4 peptides. On the contrary, the radii of W4R4 and W4H4 increased significantly ($p < 0.01$) in the presence of bDNAs (Figures 5A, 5B, and S14A). The observed results confirmed the interaction between linear peptides and bDNAs and further motivated us to study the native charge of the peptide-bound bDNA complexes. The negative charge of bDNAs perturbs the overall surface charge of linear peptides, except for W4R4 (Figures 5C, 5D, and S14B). Although the His of W4H4 binds to bDNAs, the His persists in the center of the complex, and the bDNAs form a concentric ring around it, thus generating a negatively charged group on the surface having a block type of binding. On the other hand, Arg of W4R4 binds to the bDNA in a manner where the positive charge of Arg residues surrounds the bDNA.

Structural stability of peptide-bound DNA nanostructures in denaturing conditions

Since W4R4 and W4H4 peptides bind to bDNAs in distinct ways, the presence of linear peptides can influence the relative stability of bDNAs. The maximum peak intensity for the bDNAaso was observed

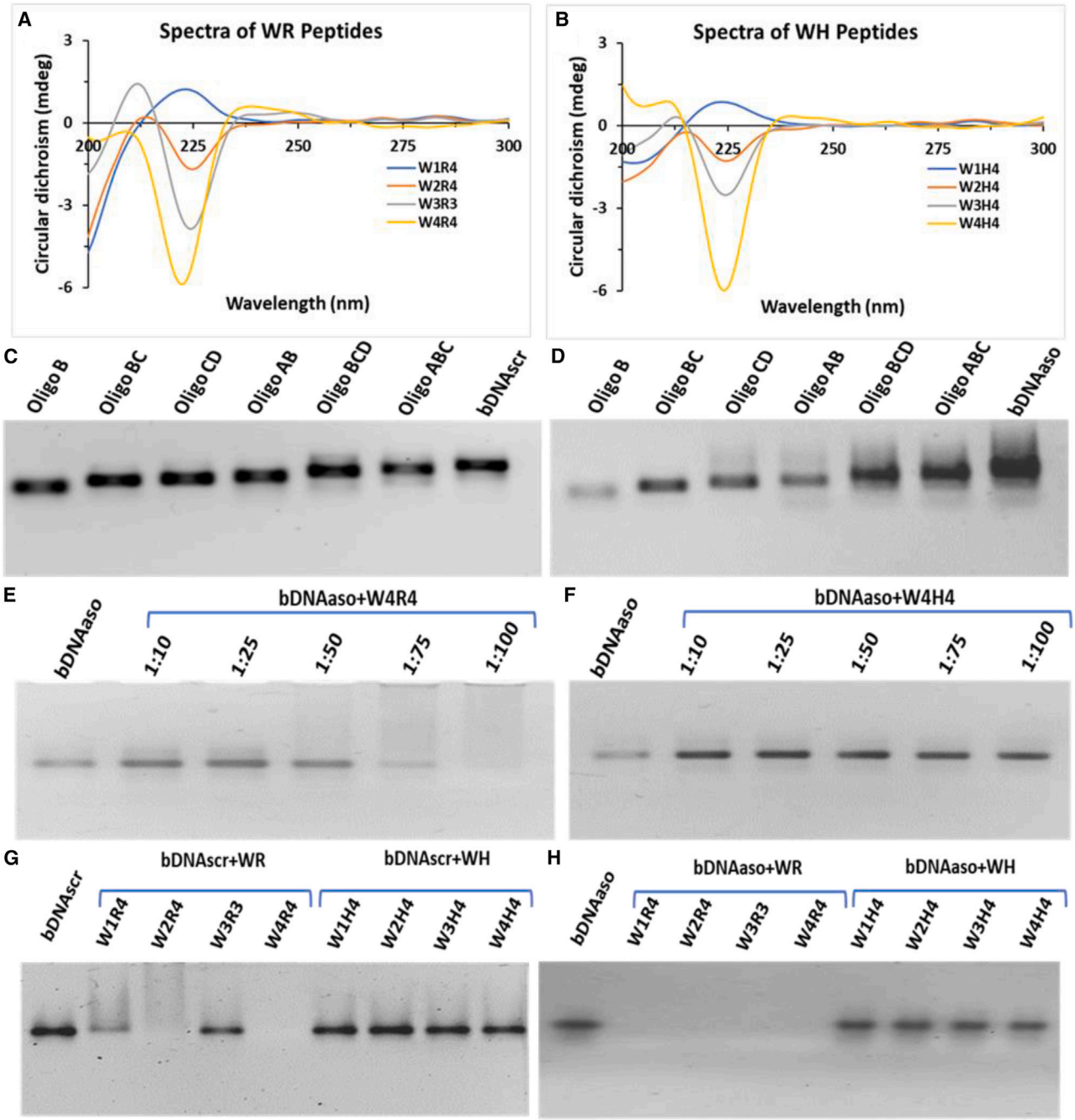

Figure 2. Characterization and binding analysis of linear peptides with bDNAs (bDNAscr and bDNAaso)

Secondary conformational analysis of linear peptides using CD spectroscopy. The negative peak confirmed the secondary conformation at 225 nm for 100 μM WR series (A) and WH series (B) peptides. However, linear peptides W1R4 and W1H4 lack peaks at 225 nm. Self-assembled bDNAscr (C) and bDNAaso (D) were characterized in 3% agarose gel electrophoresis (AGE). The composition of each oligonucleotide is labeled on the top of each lane. The differential migration was observed for individual oligos (oligo B), di-oligo complexes (oligo BC, CD, and AB), tri-oligo complexes (oligo BCD and ABC), and monomeric bDNAscr and bDNAaso structures. A homogeneous and non-spurious product of self-assembled bDNA was noticed with a clear band. Gel-shifting analysis for the development of complexes between linear peptides and bDNAs. A gel retardation experiment was conducted to assess the binding affinities of linear peptides (W4R4 and W4H4) with bDNAaso nanostructures. The bDNAaso with different w/w ratios of linear peptides (10, 25, 50, 75, and 100) were used and presented using the gel (E and F). Similarly, a 2% AGE was used to analyze the binding affinity of WR/WH peptides with bDNAscr and bDNAaso complexes. The bDNAs were incubated with peptides at a molar ratio (w/w) of 1:100 (G and H). Lane 1 primarily consists of bDNA, lanes 2–5 have WR series with bDNA, and lanes 6–9 contain WH series with bDNAs. The WR peptides have a greater binding affinity with bDNAs than the WH peptide sets.

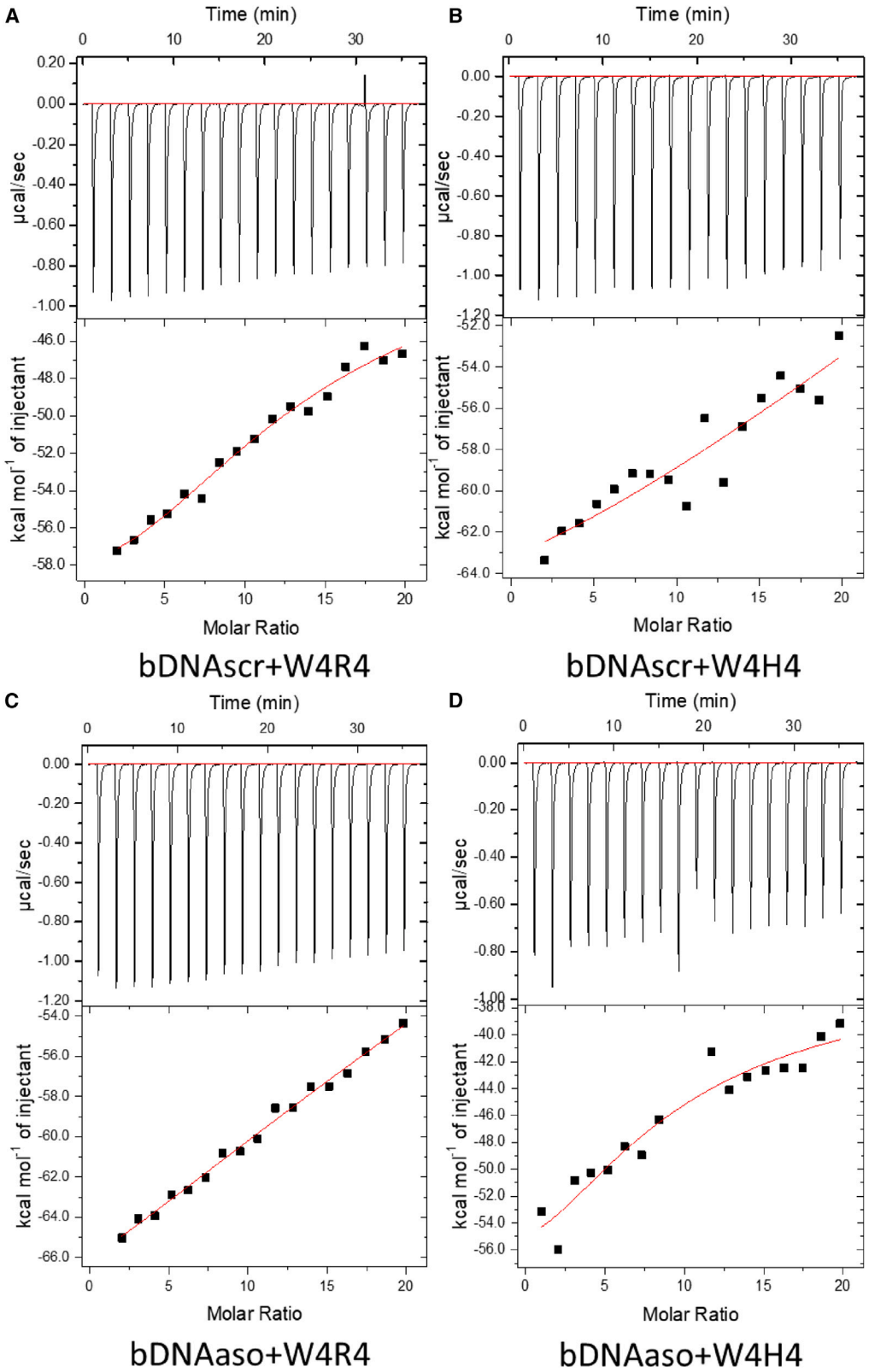

(legend on next page)

at 241 and 267 nm with the thermal melting of ~70°C (Figures S15A, and S17A). As expected, the denatured bDNA refolded back to the native B-form with an equal T_m value during the annealing process (Figure S15B). Similarly, melting curve analysis of bDNAaso was investigated in the presence of 25 μM W4R4 peptides and the T_m value was calculated to be ~80°C. However, the thermal melting of the W4H4-bound bDNAaso complex was 75°C. Similar outcomes were observed for the bDNAscr in the presence and absence of linear peptides (Figures S16 and S18). Interestingly, bDNA reoriented back to its native B-form in the presence of W4H4 peptides during the annealing process with the same T_m values in contrast to W4R4 peptides. Possibly, the binding between W4R4 and bDNA is more stable than W4H4-bDNA complex.

Further, we investigate the stability of peptide-bound bDNAs in the presence of DNase I. Initially the stability of bDNAs was determined in the presence of 10 U/mL DNase I at variable time intervals up to 30 min (Figure S19A). The control bDNAs are sensitive in the presence of 10 U/mL of DNase I and approximately 50% degradation was noticed after 30 min of incubation. Interestingly, the peptide/DNA complexes of the W3R3/W4R4-bDNA complex retained the stability in the presence of DNase I (Figure S19B). Further, in the absence of peptides, the particle sizes of the bDNAs decreased significantly ($p < 0.005$) in the presence of DNase I (Figure S19C). However, the particle sizes of peptide-bound bDNAaso remained unaltered in the presence of DNase I (Figure S19D). It has been observed that peptide-bound DNA complexes formed by W4R4 have a higher ability to preserve their native state than W4H4 peptides. Interestingly, in the presence of W4R4, bDNA complexes retained 65% of products in the presence of DNase I (Figure S19B). However, in the presence of W4H4, the bDNA is degraded close to the control (Figures S19E and S19F). Further, the structural stability of bDNAaso has been examined in 10% fetal bovine serum (FBS) in the presence and absence of W3R3 and W4R4 peptides. The relative intensity of bDNAaso remained stable for 12 h, while it gradually degraded over a period of 48 h at 37°C (Figure S20A). However, peptide-bound bDNA complexes are stable in the presence of nuclease even up to 48 h (Figures S20B and S20C).

The release of bDNAaso from W4R4 peptides complexes was examined in the presence of protease enzymes and ionic species. The control bDNAaso showed a sharp band, while the peptide-bound bDNAs exhibited the disappearance of the band, confirming the formation of the complex (Figure S21A). Interestingly, SDS and trypsin triggered the release of bDNA from the peptide complexes, while proteinase K degraded the complexes, resulting in a smeared product. However, bDNAaso bands remained intact after incubation in different protease enzymes and ionic species (Figure S21B). These results confirmed an anionic and trypsin-mediated release of bDNA from the peptide complexes in the cellular environment.

Cytotoxicity and cellular uptake study

The cytotoxicity of WR and WH peptides was tested at 2.5, 5, and 10 μM concentrations for 24 h (Figure S22). All the peptides showed a cell viability of about 90%. Further, the lactate dehydrogenase (LDH) assay was conducted to assess the toxicity and membrane leakage of cells treated with peptides. LDH is an endogenous enzyme that is ubiquitous in all cells and is extruded into the cell culture medium upon disruption of the plasma membrane. Thus, the LDH assay serves as a measure of membrane leakage and cellular toxicity. In this study, the HCT-116 cell line was used to evaluate the membrane integrity of different peptides at two different concentrations (5 and 50 μM). Additionally, the cytotoxicity of the peptide-bDNA complex was examined along with the lysed cells as a positive control. Remarkably, no significant increase in cytotoxicity was observed for either peptides alone or peptide-bDNA complexes following 24 h of exposure to the treated cells (Figure S23). These results indicated that the linear peptides and their complexes do not induce cytotoxic effects on the cells under experimental conditions.

The fluorescence microscopy experiments were executed to check the subcellular localization of peptides/Alexa 488-labeled bDNAs complexes in HCT-116 cells. The internalization of Alexa 488-labeled bDNA is negligible in the absence of the delivery vehicle (Figures 6, S24, and S25). On the other hand, substantial cellular uptake of Alexa 488-labeled bDNA was noticed in the presence of W3R3 and W4R4 inside the cytoplasm (Figures 6 and S24). However, in the case of the WH series, no such cellular internalization was observed (Figure S25). Although the WH peptide series can form a self-assembled nanostructure, the net positive charge may not be sufficient to bind with bDNAs compared to W3R3 and W4R4 sets.

Further, cellular internalization of Alexa 488-labeled bDNA was quantified in HCT-116 cells by fluorescence-activated cell sorting (FACS). This analysis indicated significant fluorescence intensity in cells treated with Alexa 488-labeled bDNA-W3R3 or W4R4 complex compared to the Alexa 488-labeled bDNA alone. For instance, W4R4 and W3R3 peptides were found to be responsible for 12.5% and 7.1% of cellular internalization of Alexa 488-labeled bDNA, respectively (Figure S26). Nevertheless, a 1.7 fold higher cellular internalization was observed in W4R4 compared to W3R3 (Figure S26B). Thus, the present finding confirms the efficiency of W4R4 as a promising carrier for bDNA delivery.

VEGF gene silencing using peptide-DNA composite nanomaterials

Around 50 nM bDNAscr and bDNAaso were transfected with the support of 5 μM peptide into the HCT-116 cell line and incubated for 4 h. Moreover, the efficacy of the selected peptides was compared to the standard Lipofectamine 2000. The mRNA expression level

Figure 3. Thermodynamic binding studies of linear peptides with bDNAs

The thermodynamic study confirmed the binding affinity of the peptides with bDNAscr (A and B) and bDNAaso (C and D). The W4R4 binds with bDNAscr and bDNAaso in (A and C), and the W4H4 with bDNAs in (B and D). The molar ratio of bDNAs in the presence of peptides has been kept constant.

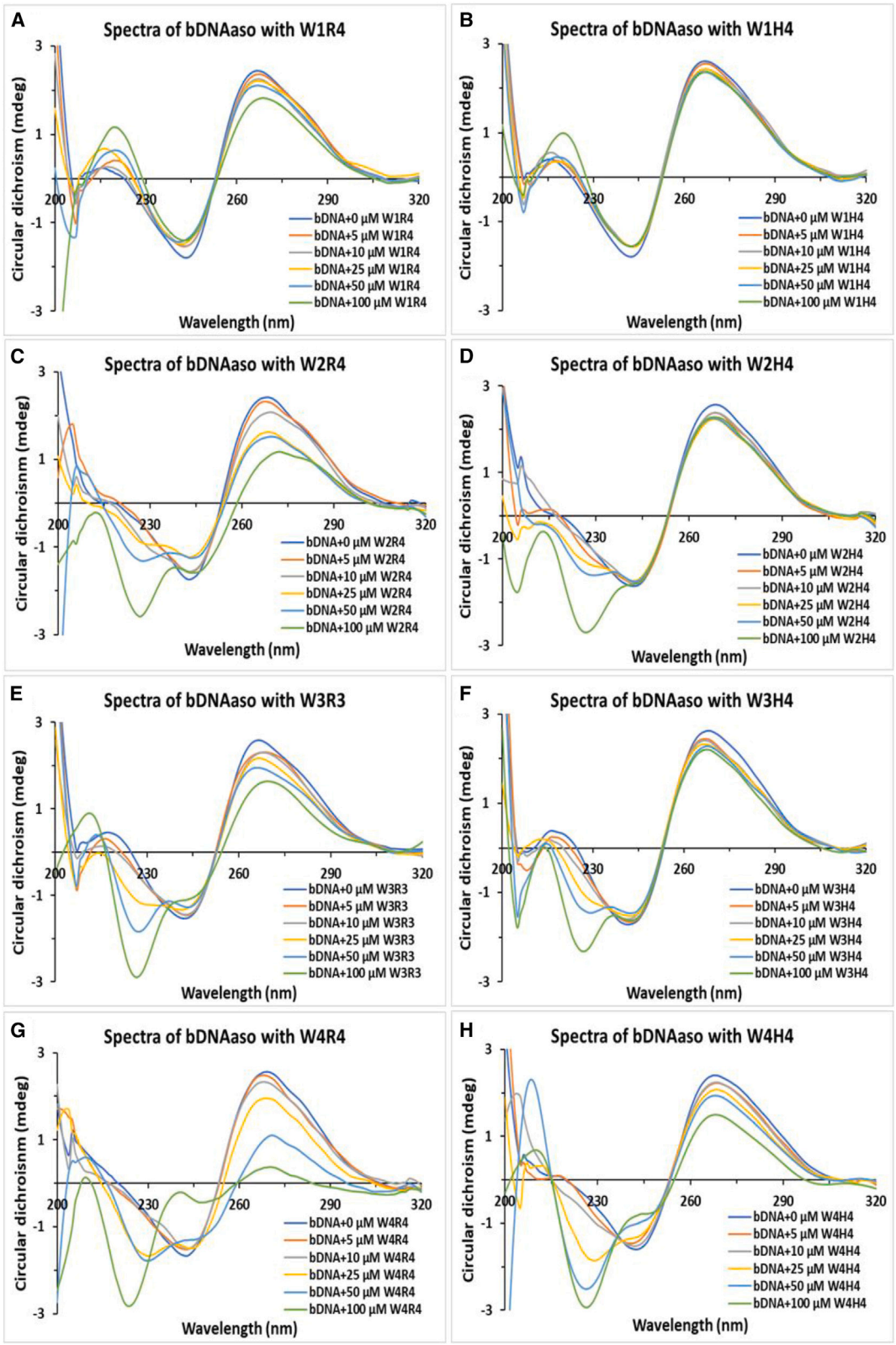

(legend on next page)

indicated that W4R4-bound bDNAaso downregulates 2.63 fold ($p < 0.001$) of VEGF mRNA expression compared to the control (Figure 7). However, the Lipofectamine-induced bDNA transfection reduced VEGF mRNA expression by about 1.47 fold ($p < 0.001$). As expected, the expression of 18s rRNA was unaffected by the presence of peptide-bDNAaso complex (Figure 7). All other WR and WH peptide-bound bDNAaso demonstrated non-significant levels of VEGF expression relative to the control groups. Similarly, protein expression was reduced by 4.35 fold in response to W4R4 bound bDNAaso complexes compared to control (Figures 7E–7H and S27). Lipofectamine 2000-based transfection of bDNAaso indicated 2.1 fold downregulation of VEGF protein expression (Figures 7G and 7H). The results clearly suggest the potential use of W4R4 peptides as bDNA carriers for the downregulation of VEGF gene expression.

DISCUSSION

Linear peptides of two different amphiphilic classes have been synthesized. Herein, the positively charged L-Arg and L-His comprise the hydrophilic heads, while the hydrophobic L-Trp is incorporated into the tails and L-Gly in varying proportions (Table S1). In order to enhance the flexibility and confer increased amphipathic properties, these novel linear peptide sequences were selected based on our earlier reports.[26,27]

The dense clustering of both peptide sequences is facilitated by the presence of hydrophobic Trp residues, which are well known for their involvement in hydrophobic-driven self-assembly.[26] Additionally, Arg residues are responsible for participating in inter- and intramolecular hydrogen bonding present in the proposed sequences. The amide bonds of peptide and proteins provide two characteristics of electronic transitions in CD spectroscopy, such as $n\pi^*$ transitions at 220 nm and $\pi\pi^*$ transitions near 190 nm. All the linear peptides except W1R4 and W1H4 peptides correlate to $n\pi^*$ transitions that denote the β-turn signature of polypeptides.[38] The β-turn motif is the third most common secondary structure found after the α helices and β sheets present in the cellular milieu. Furthermore, the β-turn motifs play an important role in the folding of globular proteins and binding to the G-protein-coupled receptors (GPCRs).[39] Moreover, transmembrane proteins such as GPCRs are responsible for most cellular responses triggered by diverse extracellular stimuli.[40–42] Thus, the β-turn motifs of linear peptides might help in easier delivery of the bDNA nanostructures.

The amphipathic nature of the linear peptides is attributed to the presence of hydrophobic tryptophan residues and hydrophilic arginine/histidine residues.[43] Moreover, optimum hydrophobic and hydrophilic balance in the sequence leads to the formation of self-assembled nanostructures. Further, the self-assembly of peptides could be correlated with previously reported WR peptides, including CPS1, CPS2, and CPS3, which have been elucidated through in silico analysis, as well as atomic force microscopy (AFM) and HR-TEM studies.[24] The hydrophobicity in the peptide sequences plays a critical role in the self-assembly process.[24] Moreover, there are no cysteine molecules in the WR and WH peptides to form disulfide linkages. Therefore, the self-assembled peptide nanostructures rely primarily on weaker interactions, including hydrogen bonds and electrostatic, hydrophobic, and intermolecular interactions. These interactions collectively contribute to the formation of stable and well-defined peptide nanostructures.

The zeta potential of the linear peptides was found to be in the range of +5 to +20 mV. These positive values on the surface could induce more affinity toward negatively charged macromolecules such as DNA.[44] However, a differential binding affinity of peptides for the bDNAscr and bDNAaso was observed in the retardation study. Further the selective binding between peptide and DNA was characterized using UV-visible (UV-vis) spectroscopy. Similar to the hypochromic effect of peptides in DNA nanomaterials,[45,46] a significant hypochromacity at 495 nm was observed for Alexa 488 bDNA with increasing concentrations of W4R4 peptide. This observation indicates that the interaction between W4R4 peptides and bDNA initiates at a molar ratio of 25:1, obtaining a maximum level of interaction at the molar ratio range of 100:1. Thus, W4R4 peptides are efficiently binding to bDNA as compared to W4H4 peptides. The Arg-rich peptides may interact strongly with bDNAs and inhibit the intercalating sites of ethidium bromide. Furthermore, guanidium groups of the Arg-rich peptide interact directly with the phosphate backbone of bDNA. Due to the interaction of guanidium groups, the hydrophobic linear peptides interact with the nucleotide bases of DNA to form hydrogen bonds. Similarly, the indole rings of Trp interacted with the guanine groups of DNAs.[47] However, the imidazole ring of His interferes with the coupling of hydrogen bonds between nucleotide bases and hydrophobic regions of linear peptides. As a result, the disappearance of the band is expected in the case of Arg-rich peptides. Similar outcomes were also seen in siRNA or ASO sequences during interactions with cyclic peptides.[24] As mentioned earlier, the guanine-rich overhang regions in the bDNA can form hydrogen bonds with the guanidinium group of the Arg of linear peptides.[48] The current data suggest that bDNAaso efficiently interacts with Arg-rich linear peptides. The negative enthalpy and entropy values of ITC suggest that bDNAs interact with all the linear peptides in non-covalent binding modes (Figure S12). The negative values claim that the interaction was primarily by hydrogen bonds and van der Waals forces of interaction, which may be attributed to proton exchange between the peptides and bDNA.[49] These thermodynamic characteristics suggest a favorable exothermic interaction between peptides and bDNAs (Table S4). CD spectroscopy was also conducted to assess the

Figure 4. Binding conformation of bDNAaso in the presence of linear peptides

The CD spectra of a B-DNA show distinctive peaks at 267 nm and 241 nm. The bDNAaso interacts with WR peptides (A, C, E, and G) and WH peptides (B, D, F, and H). The bDNA concentration was kept at 1 μM and was titrated with different molar concentrations (0–100 μM) of linear peptides. The peptides of the WR series demonstrate a higher binding affinity for bDNAs than the WH series.

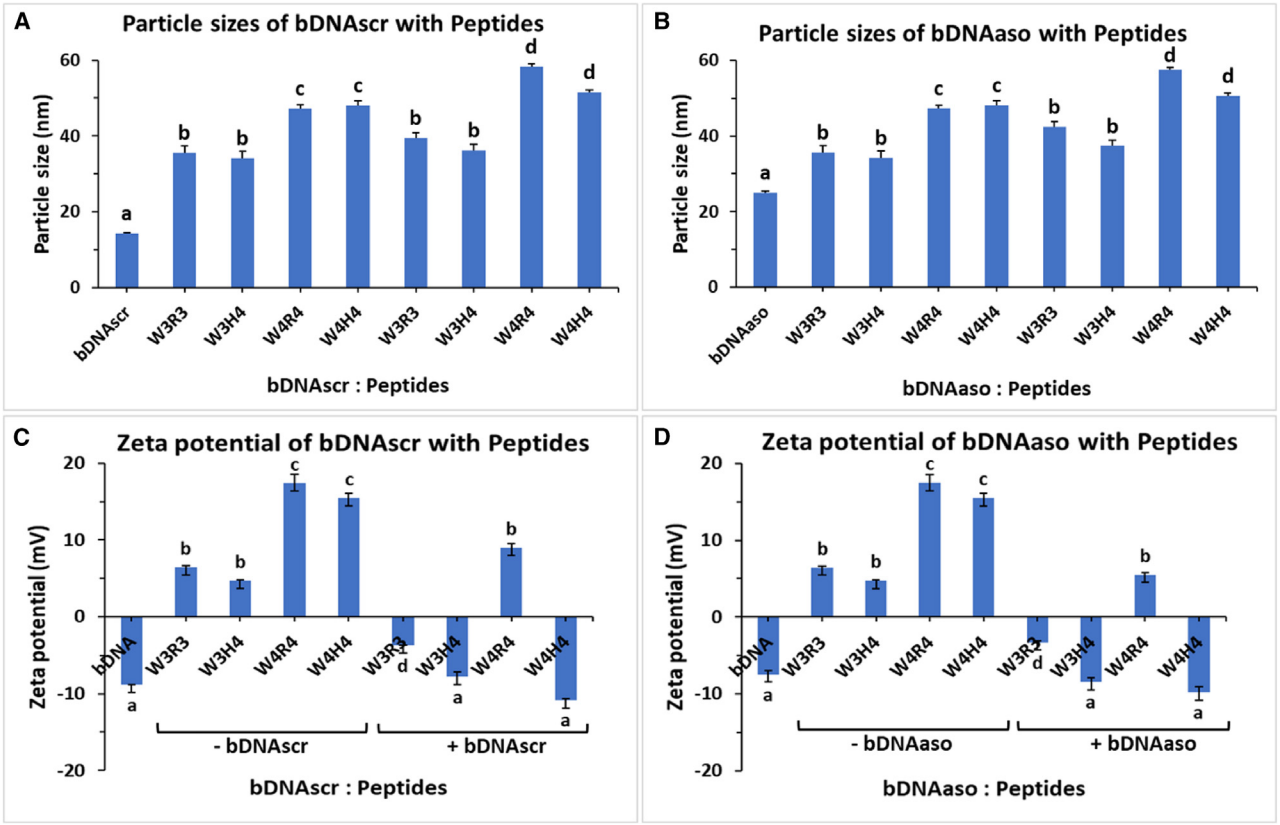

Figure 5. Particle size and zeta potential analysis of peptide-bound bDNAs

The particle sizes of bDNAs and peptides demonstrate the development of nanometer-range complexes. The figure represents the particle size of bDNAscr and peptide-bound bDNAs (A) and bDNAaso and peptide-bound bDNAs (B). The findings support the formation of peptide-bound bDNA complexes. The zeta potential confirms the direct interaction of peptides with bDNA nanostructures. The surface charges of bDNAscr and bDNAaso were differentially influenced by peptides (C and D). Interestingly, in the presence of W4R4, the bDNA shows positive zeta potential, which may help in DNA transfection. Data with superscripts are significantly different at $p < 0.05$.

secondary conformational changes of bDNA in the presence of peptides. Our results suggested that positively charged linear peptides might bind arbitrarily to the phosphate backbone of bDNAs. The flattened peaks of the bDNA monomers might be due to the "slide" or "hop" of linear peptides binding to the nucleotide bases.

Light-scattering studies were conducted to evaluate the surface charge and size of the peptide-bound bDNA complexes. The experimental radii of bDNAs are almost identical to the theoretical values of bDNA nanostructures calculated from the B-form of DNA with Watson and Crick base pairing.[50,51] Nevertheless, the size of peptides is increasing in the presence of bDNAs. These experimental findings have further supported the interaction of linear peptides with bDNAs. Similar findings were observed for the catalase in the presence of bDNAs.[52] Further, the surface charge of peptides was examined in the presence of bDNA nanomaterials. Linear peptide-bDNA complexes were reported to exhibit negative surface charges like liposome-mediated-DNA clusters.[53] However, a positive surface charge was noticed for the W4R4 peptide-bDNA complex. Although the W4R4 peptide primarily maintained an overall positive charge, the hydrophilic head of the Arg encapsulated the bDNAs between two or more W4R4 peptides, thus forming a micelle structure. Interestingly, the 1,2-dioleoyl-3-trimethylammonium propane (DOTAP):cholesterol liposome-mediated interaction with supercoiled DNA yielded similar findings.[54] These observed results concur with secondary conformational data that W4R4 bound to bDNAs and confirmed a stable complex formation between the peptide and bDNAs.

The stability of these peptide-bound DNA complexes under varying denaturing conditions is a crucial factor in determining their durability in physiological environments. The observed T_m value of W4R4-bound bDNAaso is higher in comparison to the bDNA alone due to encapsulated bDNA between the linear peptides. However, the T_m of bDNA decreased to 65°C during the thermal renaturation because positively charged Arg hindered the refolding back of the phosphate backbone. A similar annealing pattern was also observed for lanthanum-induced Z-DNA, where lanthanum binds strongly to the phosphate backbone and grooves.[55] The improved thermal stability of bDNAs in the presence of linear peptides is reflected through

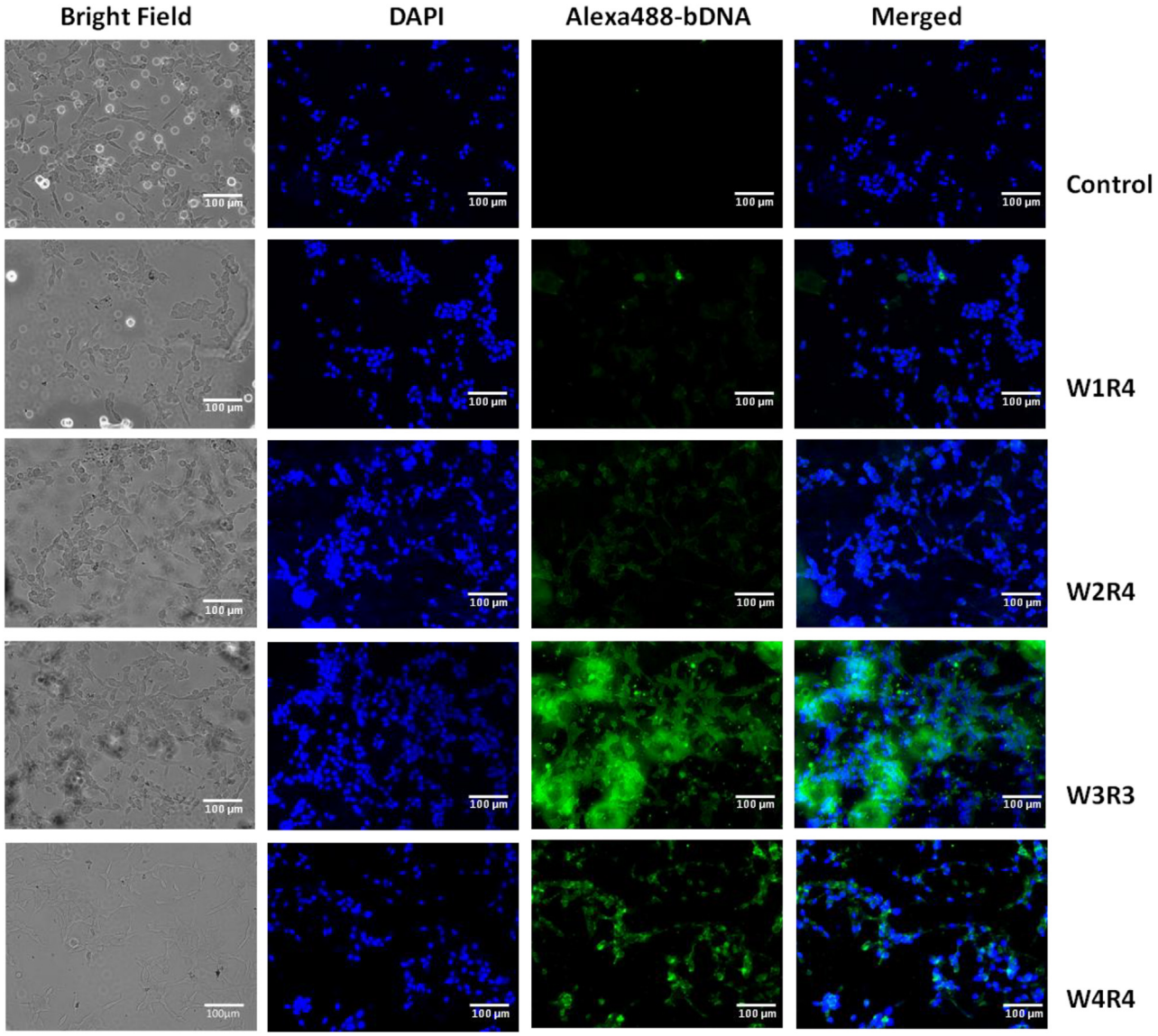

Figure 6. Fluorescence microscopy images of Alexa 488 bDNA

The uptake of Alexa 488 bDNA in HCT-116 cells in the presence of W1R4, W2R4, W3R3, and W4R4 and stained with DAPI. It has been observed that the internalization of Alexa 488-labeled bDNA is negligible for control and WR sets. A substantial cellular uptake was noticed for W3R3 and W4R4 peptide-bound bDNAs.

spectroscopic and thermodynamic investigations. The W4R4-peptide-bound bDNA is found to be the most stable due to its unique complexation ability.

DNA-based nanoparticles are biodegradable with a half-life of a few hours due to several factors that limit their functional applicability.[56] Meanwhile, DNase I was found to be the predominant nuclease in mammalian serum, with an average DNase I activity of 1.49 U/mL.[57] Results suggested that bDNAs are only sensitive to 10U/mL DNase I activity ($p < 0.01$). Similarly, nuclease susceptibility was reported for the bDNAs in the presence of DNase I.[36] Nevertheless, Arg-rich peptides are able to protect the bDNAaso against the activity of DNase I. Additionally, the nuclease stability of bDNA nanostructures was examined in the presence of FBS, which contains ~256 U/L of DNase I.[2] The results indicate that peptide-bound bDNA structures exhibit complete stability for 48 h in cell culture media, in contrast to the 25% stability observed in naked bDNAs. Based on our observations, we hypothesize that these peptide-bound bDNA structures confer enhanced structural stability. Therefore, these findings indicate that the Arg-rich peptides minimize the binding and protect against the enzymatic activity of endonucleases. In contrast, W4H4 peptide-bound bDNAs exhibited 20% protection against

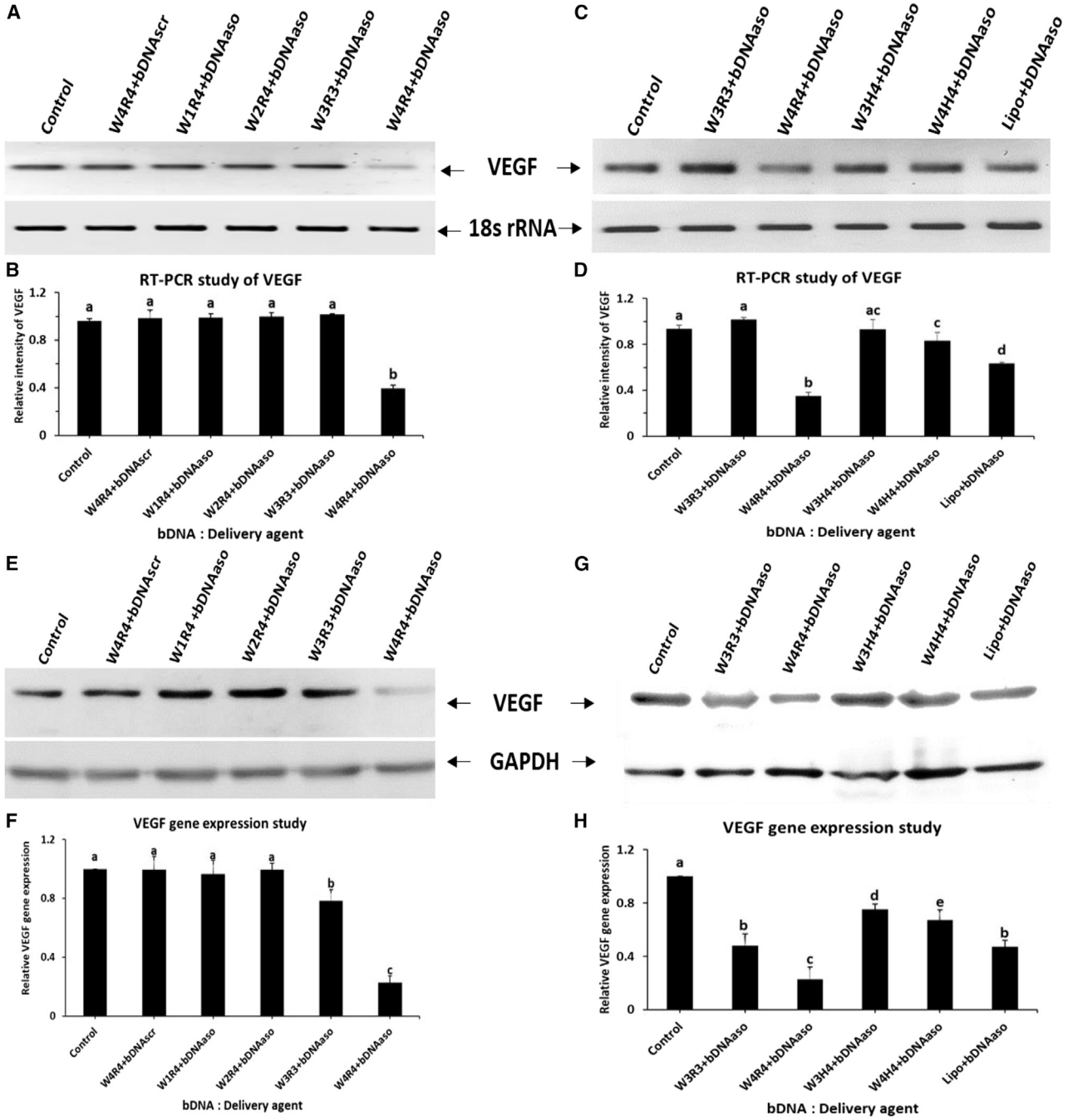

Figure 7. Quantification of VEGF at transcriptional and translational levels

The transfection efficacy was investigated with 50 nM bDNAaso nanostructures and normalized using 18S rRNA (A–D). The effect of bDNAaso was compared to bDNAscr and Lipofectamine 2000. Western blots of VEGF protein expression relative to GAPDH protein expression for bDNAaso delivery via W1R4, W2R4, W3R3, and W4R4 (E). Quantifications of VEGF protein expression with respect to the control GAPDH (F). The VEGF protein expression gel image was relative to GAPDH for bDNAaso delivery via W3R3, W4R4, W3H4, W4H4, and Lipofectamine 2000 (G). Quantifications of VEGF protein expression against control GAPDH (H). Data shown here represent the mean ± SD of triplicates. The level of significance was determined by one-way ANOVA followed by Duncan's new multiple-range tests. Data with superscripts are significantly different at $p < 0.05$.

nuclease degradation like the control bDNAs (Figures S19 andS20). Therefore, we propose that Arg-rich peptides encapsulate bDNAs within the hydrophobic regions of the peptides, leading to enhanced structural stability and protective activity. Based on these findings, Arg-rich peptides are considered superior transfecting agents compared to His-bearing peptides.

The stability of the complex between the W4R4 peptide and bDNAaso is crucial for potential therapeutic applications. However, the mechanism of release of bDNAs from the complex remains unclear. Serum nucleases have been reported to degrade nucleic acids with a half-life of up to 4 h, while protease enzymes such as proteinase K and trypsin can digest carboxyl groups of amino acids such as Arg, Gly, and Trp.[35,58] The stability and release of bDNA biomaterials from the complex were examined in the presence of trypsin, proteinase K, sodium chloride (NaCl), and SDS.[59,60] The complexes were stable in all conditions except for trypsin and SDS. The presence of high-density cationic charges in the complex imparts stability under polyelectrolyte conditions, enabling efficient transfection of peptide-bound bDNAs into cells.[24,61] However, the release of bDNAaso in the presence of the proteolytic release and anionic species such as SDS signifies a trypsin-mediated or ion-induced release inside the cells. Gel analysis showed that bDNAs were stable in the presence of trypsin, proteinase K, NaCl, and SDS in the absence of linear peptides.

The cytotoxicity of various linear peptides was evaluated in HCT-116 cells through the MTT assay. The cells were observed to be 90% viable in the presence of 10 μM linear peptides. Similarly, the results of the LDH assay indicated that linear peptides and their complexes do not induce cytotoxic effects on cells under the experimental conditions. As a result, all linear peptides have been investigated to deliver bDNAaso inside the cell. In order to check the internalization efficiency of the peptides, intracellular uptake of Alexa 488-labeled bDNAs was investigated. These observations indicate that self-assembled peptide nanostructures with sequences W3R3 and W4R4 exhibited higher efficiency in transfecting bDNAs into the cellular environment. This observation was also supported by the FACS study.

The transfected cells with the bDNAaso were incubated for 48 h in complete medium to evaluate the inhibition of VEGF expression. The results indicated that W4R4-bound bDNAaso downregulates 2.63 fold of VEGF mRNA expression compared to the Lipofectamine-induced bDNA transfection by about 1.47 fold. All other WR and WH peptide-bound bDNAaso demonstrated a non-significant level of VEGF expression compared to the controls. These findings are consistent with our previous study, where we demonstrated the effective suppression of VEGF expression using a cyclic peptide-bound siRNA complex.[24] Due to the positive zeta potential of the Arg-rich linear peptides, W4R4 peptides were found to deliver bDNAs inside the cells and suppress VEGF expression more effectively than Lipofectamine.[62] Thus, the efficacy of suppressing VEGF expression is 2 fold greater in the case of W4R4-bound bDNAaso than Lipofectamine-bound bDNAs. Thus, peptide-bound bDNA complexes were found to be superior for reducing mRNA levels than naked bDNAs due to their more efficient transfection and stability inside cells. Similarly, western blotting was utilized to evaluate protein expression in cells transfected with a peptide-bDNA complex. Protein expression was reduced by around 4.35 fold using W4R4-bound bDNAaso complexes, as compared to 2.1 fold downregulation using Lipofectamine 2000-bound bDNAaso complexes. The expression of VEGF at the protein level suggests that the efficiency of the W4R4 peptide in delivering DNA is much higher than the widely used Lipofectamine 2000. Based on this finding, the protective ability of peptide nanostructures toward the transfection of nucleic acid therapeutics is confirmed.

In summary, this report describes for the first time the effective delivery of bDNA nanostructures using linear peptides. Moreover, an efficient and simple method has been developed for delivering bDNA nanostructures that carry therapeutic molecules such as miRNA, anti-miRNAs, siRNAs, and ASOs. The present study also reveals that bDNA nanostructures carrying antisense VEGF could be delivered successfully by W4R4 peptide, resulting in downregulation of VEGF at post-transcriptional and post-translational levels. The biophysical investigations confirmed the binding of peptides to bDNA, thus enabling the transfection of the bDNAs-peptide complex. Nevertheless, these peptide-mediated deliveries of bDNAs can target mRNAs more effectively than Lipofectamine 2000. This peptide-based biomolecular delivery strategy opens a new route to deliver therapeutic nucleic acids.

MATERIALS AND METHODS

Chemicals and reagents

Molecular-grade Tris, SDS, glycine, Coomassie brilliant blue R250, ethanol, and methanol were bought from MP Biomedicals, and polyvinylidene fluoride (PVDF) membranes from Millipore (MA, USA). Fmoc-amino acid trityl chloride resins, Fmoc-L-amino acid, coupling chemicals, and 2-(1H-benzotriazole-1-yl)-1,1,3,3-tetramethyluronium hexafluorophosphate were bought from Chempep (Miami, FL). Na_2EDTA, skim milk, FBS, MTT, NaCl, $KHPO_4$, KCl, and $NaHPO_4$ were bought from Himedia (India). The chemicals such as agarose, Trizma base, magnesium acetate, acetic acid, EDTA, ethidium bromide and 6× loading dye were purchased from Sigma-Aldrich. NexGen HM Protease inhibitor (BPOI001) was bought from Biopioneer (India). SRL Chemicals (India) supplied the reagents, such as N, N-dimethylformamide (DMF) and N,N-diisopropylethylamine (DIPEA). Polypropylene columns were supplied by Bio-Rad. Lipofectamine 2000 was purchased from Thermo Scientific. The LDHFSR-01 kit was procured from Meril Diagnostics. VEGF antibody (sc-365578), and VEGF siRNA (sc-29520) were purchased from Santacruz. GAPDH monoclonal antibody (10-10011) and alkaline phosphatase-conjugated goat anti-mouse immunoglobulin (Ig) G (11-302) were purchased from Abgenex. 18s rRNA primer and VEGF primer (Table S3) were custom synthesized from Integrated DNA Technology (IDT), USA.

Synthesis of peptides

All the peptides were synthesized by solid-phase peptide synthesis. The synthesis procedure of amphipathic peptides was performed as

per the reported articles.[26] All peptide-related reactions were carried out at room temperature in polypropylene columns by physical mixing with a vertical rotator. In a nutshell, all peptides were produced utilizing the SPPS method and Fmoc chemistry. HBTU and DIPEA were used as coupling and activating agents, respectively. Deprotection of Fmoc at every stage was performed by utilizing 20% v/v piperidine in DMF. The peptide-attached resins were shaken for 2 h with a 15-mL solution of trifluoroethanol (TFE), acetic acid, and dichloromethane (DCM) in a ratio of 2:2:6 (v/v/v) to detach the side-chain-protected peptides from the solid phase. By the process of filtration, resin and peptide solution were separated. A rotary evaporator was used to obtain the dry-side chain-protected peptides. In a ratio of 90:5:2:3, trifluoroacetic acid (TFA)/thioanisole/anisole/1,2-ethanedithiol (EDT) reagents were used for the side-chain deprotection over 2 h. The unpurified peptides were precipitated by adding 75 mL of cold diethyl, and they were then purified using a gradient system on an Agilent 1260 infinite Quaternary LC system reversed-phase column.

Characterization of peptides by mass spectrophotometer and HR-TEM

MALDI-TOF mass spectrometry at the Proteomics facility, Institute of Life Sciences, Bhubaneswar (AB SCIEX TOF/TOFTM 5800 System) was used to determine the mass of the peptides of the purified peptides and the matrix CHCA was used, and the matrix mixed peptides were dropped in the MALDI plate and given time to dry. The self-assembled nanostructure of 2 mM WR and WH series of peptides was prepared in an aqueous solution and kept for 2 days at 25°C–30°C. Ten-microliter samples were placed into the 300-mesh formvar-coated carbon TEM grid and incubated for 2 min. The peptides were stained with 20 μL of 2% uranyl acetate applied to the TEM grid and incubated for 2 min at room temperature. The additional stain was removed using filter paper, and TEM grids were kept at room temperature for 24 h to completely dry. The images were taken with a field emission gun transmission electron microscope 300 kV (using the facility at IISER, Mohali).

Designing of bDNA nanostructures with antisense sequences

Oligonucleotides (oligo B, C, A-scr, D-scr, A-aso, and D-aso) were used in an equimolar stoichiometric ratio to form different bDNA nanostructures (Table S1). As mentioned earlier, the internal and external hybridizing regions of bDNA were derived from catalase, SOD1, and SOD2 genes of *Rattus norvegicus*.[33] In the case of the bDNAscr, the overhang (A-scr and D-scr) were replaced with scramble sequences.[35] The overhangs (A-aso and D-aso) of bDNAaso were replaced with the ASO sequences to target the VEGF gene.[24] These designed oligonucleotides were procured from IDT and used in experimental studies without additional purification and modifications.

Self-assembly and characterization of bDNA

The synthesized oligonucleotides were self-assembled in TAEM buffer, which contains Tris base (40 mM, pH 8.0), acetic acid (20 mM), EDTA (2 mM), and $Mg(Ac)_2$ (12.5 mM) by a single-pot synthesis approach in a thermal cycler (Bio-Rad, S-1000). The bDNAs were self-assembled using four oligonucleotides in an equimolar ratio. The reaction mixture of bDNA was denatured at 95°C for 9 min and then slowly cooled down to 4°C at a rate of 0.3°C/s.[33] All reaction mixtures were performed five times with the final concentration of 1 μM, and the self-assembled DNA nanostructures were stored in aliquots at −20°C until further use. The bDNAs nanostructures were characterized using 3% AGE at a constant voltage of 80 V for 25 min in 1× TAE running buffer.

A gel-shifting assay was performed to demonstrate the preferential binding of the linear peptide with bDNAs. A 20-μL mixture containing 1 μM bDNAaso/Alexa 488 bDNA and a w/w ratio (10, 25, 50, 75, and 100) of W4R4 and W4H4 linear peptides was prepared and incubated at room temperature for 1 h. The mixture was subsequently electrophoresed using 2% AGE. Similarly, the reaction mixture comprised 100 nM bDNAs and 10 μM linear peptides. The final volume was made up to 20 μL with the self-assembly buffer. These samples were incubated at room temperature for 1 h and then electrophoresed in horizontal gel electrophoresis (H99X, Hoefer) using 2% AGE for 25 min at a constant voltage of 80 V. All the gel images were documented in the FluroChem E system (Cell Biosciences).

Absorbance study of Alexa 488 bDNAs with linear peptides

Alexa 488-labeled bDNAs (1 μM) were incubated for 1 h at 25°C with increasing ratios of either W4R4 or W4H4 at peptide/bDNA molar ratios of 0:1 to 100:1, and absorbance spectra were measured using the Cary-100 UV-vis spectrophotometer (Agilent, USA) with an absorbance range of 450–550 nm. The hypochromic effect of the Alexa 488 bDNAs was quantified by the relative change in absorbance, ΔOD_r, defined as follows[37]:

$$\Delta \mathrm{O}D_r = (OD_0 - OD) / OD_0$$

where OD_0 is the initial absorbance of the free Alexa 488 bDNA and OD is the absorbance of the bDNA-peptide complexes. Plotting ΔOD_r allows the detection of interaction of W4R4 or W4H4 peptides with the bDNAs at molar ratios. The increased molar ratio of W4R4 represented a relative increase in the hypochromicity of peptide/bDNAs compared to the W4H4/bDNA complexes.

Thermodynamics of binding between bDNAs with linear peptides

The GE Healthcare MicroCal ITC_{200} was used to study the thermodynamics of binding between bDNAs and linear peptides at 25°C. The sample cell of the calorimeter was loaded with 200 μL of bDNAscr (1.0×10^{-6} M) and 40 μL 1× TEAM buffer (pH 7.4). The bDNA was titrated with 100 μM peptides using a 40 μL injection syringe with a 120 sec gap between each 1.5 μL injection for 18 injections at 500 rpm. The thermodynamic heat associated with each injection was observed as a peak that keeps the sample and reference cell at identical temperatures, and the data were plotted as integrated quantities. The thermodynamics of bDNAscr and linear peptides data were fitted and analyzed with a sequential model of one binding site using

Origin 7.0 provided by the MicroCal instrument. Similarly, bDNAaso of 1 μM was loaded in the ITC sample cell, and the thermodynamic behavior of bDNAaso in the presence of peptides was examined with similar parameters.

Secondary structure of linear peptides in the presence of bDNAs

The CD spectrophotometer (Chirascan, Applied Photophysics) was used to characterize the secondary conformational study of the linear peptides in the range of 200–300 nm with a scan rate of 60 nm min^{-1} at 25°C in a 2 mm cuvette. The MilliQ water acted as the baseline for subtracting the spectral readings. A typical reaction mixture consists of 380 μL of MilliQ water and 20 μL of LP series (2×10^{-3} M). All the spectral readings are an average of three readings.

The changes in the secondary conformation of bDNA in the presence of linear peptides were monitored using the CD spectrophotometer with a similar spectral range and parameters in a 1 mm cuvette. The self-assembly buffer acted as the baseline. A typical reaction mixture contains 200 μL of 1 μM bDNA. Subsequently, the linear peptides were added to the sample of different molar concentrations ranging from 5 to 100 μM. The Quantum Northwest TC-25 maintained the experimental temperature. Each spectrum is an average of three readings. Both the bDNAs were titrated with sets of linear peptides with an incremental addition to examine the spectral changes of bDNA.

Dynamic light-scattering measurements

The hydrodynamic diameter of linear peptides in the absence and presence of bDNAs were measured at 658 nm using a Litesizer-500 with a fixed scattering angle of 175° at 25°*C*. bDNAs were dissolved in the self-assembly buffer, pH 7.4, and filtered through a 0.22 μm sized micro-sampler. In brief, 100 μM linear peptides and 1 μM bDNAs were incubated for 1 h, whereas the linear peptide was used as a control. Each value is an average of triplicate readings. Hydrodynamic radius (R_h) was estimated based on the autocorrelation analysis of scattered-light-intensity data based on the translation diffusion coefficient by the Stokes-Einstein relationship.

$$R_h = kT/6\pi\eta D$$

where R_h is hydrodynamic radius, k is Boltzmann constant, T is temperature, η is viscosity of the water, and D is diffusion coefficient.

Zeta potential measurements

The zeta potential of linear peptides in the absence and presence of bDNAs were measured using a Univette low-volume cuvette in the Litesizer-500 at 25°*C*. For the bDNA-peptide complex, 1 μM bDNA was incubated with 100 μM linear peptides for 1 h, and then zeta potential was measured using the Litesizer-500. The control bDNA and linear peptides with respective concentrations were also incubated for 1 h at 25°*C* before measuring the zeta potential. Zeta potential (mV) was estimated based on the electric potential of the slipping plane using the Smoluchowski approximation method based on the Kalliope software. Each value is an average of triplicate readings.

Thermal melting of bDNAs in the presence of linear peptides

A thermal melting experiment was conducted using a CD spectrophotometer (Chirascan, Applied Photophysics). The thermal stability of linear peptide-bound bDNA complexes was assessed to demonstrate their high-temperature stability. The spectral range was set from 200 to 300 nm in a 1 mm pathlength cuvette, and 1× TAEM buffer solution was used as a blank for baseline correction. The thermal melting study of bDNA was done with 200 μL of 1 μM bDNAscr and 25 μM linear peptides. Similarly, bDNAaso was taken in the cuvette, and 50 μM linear peptides were added for the thermal melting study. Both bDNAs were heated at 2°C/min from 20°C to 90°C. The data were recorded at 5°C per step of temperature rise. Thermal melting of bDNAs was observed with and without linear peptides.

DNase I stability assay

In the presence of DNase I, the structural stability of DNA nanostructures was determined. The reaction mixture consisted of 20 μL of 1 μM bDNA complexes and was digested with 10 U/mL of DNase I. Similarly, 1 μM bDNAs were incubated with 100 μM linear peptides consisting of W3R3 and W4R4 to determine the stability of complexes in the presence of 10 U/mL of DNase I for 15 and 30 min. Correspondingly, 1 μM bDNAs were incubated with 50 μM linear peptides consisting of W4R4 and W4H4 peptides. Then the complexes were incubated with DNase I for 5, 10, 20, and 30 min at 37°C, and the digested products were electrophoresed in 2% AGE at 80 V for 25 min. All the gel images were documented in the FluroChem E system (Cell Biosciences). These band intensities were analyzed for the stability of the relevant complexes. Similarly, the hydrodynamic diameter of bDNAs was also measured without and with linear peptides in the presence of DNase I. In brief, 100 μM linear peptides (W4R4 and W3R3) and 1 μM bDNAaso were incubated for 1 h, whereas the incubated bDNAs (bDNAscr and bDNAaso) were used as a negative control in the presence of DNase I. All the samples were measured using the Litesizer-500. Each value is an average of triplicate readings.

Serum stability study

The stability study of bDNA structures containing ASOs in the presence of serum was conducted *in vitro* by taking 1 μM bDNAaso in 10% FBS. Similarly, a reaction mixture comprising 1 μM bDNAaso and 100 μM W3R3 and W4R4 linear peptides was incubated with 10% FBS. After mixing, the samples were incubated at 37°C for 0, 1, 4, 12, 24, and 48 h. The incubated products were then analyzed by 2% AGE at 80 V for 25 min. After electrophoresis, the gel images were obtained using the FluoroChem E documentation system, where the band intensity corresponded to the structural stability of peptide-bound complexes in serum.

Release of bDNA from complexes

A gel-shifting experiment was performed to investigate the release mechanism of peptide-bound complexes. One micromolar bDNAaso and 100 μM W4R4 in 20 μL of serum-free DMEM were incubated at room temperature for 1 h. Subsequently, to examine the release

mechanism of peptide-bound bDNA complexes, the samples were treated with 300 mM NaCl, 1% SDS, 2 nmol proteinase K, and 510 nmol trypsin for 30 min. These samples were run in the horizontal gel electrophoresis (H99X, Hoefer) using 2% agarose gel for 25 min at a constant voltage of 80 V. Gel images were captured using the FluroChem E system (Cell Biosciences).

Cytotoxicity study of peptides using MTT assay

MTT assay was used to analyze the cytotoxicity of peptides. In a nutshell, 10,000 cells in 100 μL of complete medium were seeded in 96-well plates and allowed to adhere for 24-h incubation at 37°C in a 5% CO_2 humidified environment. The cells were exposed to peptides separately at varying concentrations, including 2.5, 5, and 10 μM for 24 h under identical conditions. After the incubation period, 100 μL of 0.5 mg/mL MTT solution was added to each well and allowed to incubate for 4 h in the condition mentioned above, and the formazan formation in the wells was observed under light microscopy. Then, the MTT solution was removed from the wells without disturbing the formazan. The generated formazan crystals were dissolved in 100 μL of DMSO solution, which was added into wells and incubated for 10 min in smooth shaking conditions for complete dissolution to appear purple-blue. The color was then measured at 570 nm using a Multiskan Microplate Photometer reader. In the experiment, untreated cells were used as the negative control, and each assay was executed in triplicate. The cell viability was also calculated using the formula below in MS Excel.

$$\%\ of\ cell\ viability\ =\ [OD\ at\ 570\ nm\ of\ treated\ cells\ /\ OD\ at\ 570\ nm\ of\ control\ cells] \times 100$$

Cytotoxicity study of peptides and complexes using LDH assay

The lactate dehydrogenase (LDH) assay was employed to assess the cellular toxicity of peptides. Initially, 10,000 cells in 100 μL of complete medium were seeded in 96-well plates and allowed to attach for 24 h at 37°C in a humidified atmosphere with 5% CO_2. Subsequently, the cells were treated with different concentrations of peptides containing the WR and WH series, namely 5 and 50 μM, for 24 h under the same conditions. Furthermore, a complex of peptides, bDNA-peptide complexes, and bDNAaso was formed by mixing 8 μM peptides with 40 nM bDNAaso, which was then administered to the cells. After 24 h of incubation, cells were centrifuged at 250 × *g* for 4 min, and then 50 μL of supernatant was collected and stored at −20°C. The LDHFSR-01 kit (Meril Diagnostics) was employed for the LDH assay, utilizing two reagents: R1-LDH-P, composed of 2 mM sodium pyruvate, and R2-LDH-P, composed of 1 mM NADH. A 15-μL sample extract was added to 100 μL of the reagent, following the manufacturer's protocol.

$$\text{Pyruvate} + \text{NADH} \xrightarrow{\text{LDH}} \text{Lactate} + \text{NAD}^+$$

The decrease in absorbance was recorded at 340 nm, resulting from the conversion of NADH to NAD^+. The absorbance was directly proportional to LDH activity, which was an indicator of cellular viability.[63] Cell viability was calculated using the following formula in MS Excel:

$$\%\ of\ cell\ viability\ =\ 1\ -\ \{Experimental\ LDH\ release\ (OD340\ nm)\ /\ Maximum\ LDH\ release\ (OD340\ nm)\} \times 100$$

Cellular uptake study of bDNA by fluorescence microscopy

Herein, 1 mL of complete medium containing 2×10^5 HCT-116 cells was grown in six-well plates. The sterile glass coverslips were kept in each well of six-well tissue culture plates before the cell seeding. The Alexa 488 bDNA (0.04 nmol) was mixed with 4 nmol of peptides in 1 mL of serum-free DMEM medium and kept at room temperature for 30 min to form a peptide-bDNA complex. Then complexes were introduced to cells and incubated at 37°C in 5% CO_2 for 4 h. After incubation, medium was taken out, and cells were fixed with 4% paraformaldehyde followed by PBS wash. In 1:5,000 dilution, DAPI was added for nucleus staining. With the aid of mounting material, the coverslips were fixed. The FLoid Cell Imaging Station microscope from Life Technologies was then used to study the cells.

bDNA cellular uptake study using FACS analysis

For this, 2×10^5 cells were seeded in six-well tissue culture plates in serum-free DMEM medium overnight. Then 1× PBS was used for washing (2×) after removing medium from plates. Further, 75 nM Alexa 488-labeled bDNA was mixed with 25 μM W3R3 and W4R4 in 500 μL of DMEM and left at room temperature for around 30 min for bDNA-peptide complex formation. Then the complex was introduced into the seeded cells for cellular internalization study and incubated at 37°C overnight. Further, medium containing the complex was removed. To detach the cells from the surface of six-well plats, 0.25% trypsin/0.53 mM EDTA was added into the well and left for 5 min at 37°C, followed by washing with 1× PBS. Then the cells were collected by centrifugation at 700 × *g* for 5 min, followed by washing twice with 1× PBS. Last, 1× PBS was added to resuspend the cells and analyzed by BD FACS Cento-II. All experiments were carried out in triplicate.

VEGF expression using RT-PCR and western blot

After cells were harvested, total RNA was extracted using TRIzol reagent (Invitrogen) following the manufacturer's protocol. The RNA pellet was washed with 1 mL of ice-cold ethanol and the tubes were kept for air drying. Then 50 μL of DEPC water, 5 μL of DNase I, and 5 μL of 10× reaction buffer were added to tubes containing air-dried RNA and incubated for 1 h at room temperature. The stop solution was added to the reaction mixture and heated at 70°C for 10 min. RNA samples were reverse transcribed using the cDNA synthesis kit (K1622, Thermo Scientific) and stored at −80°C. RT-PCR (Bio-Rad, USA) was done using a gene-specific primer (Table S3) and 18S rRNA as an internal reference to normalize

gene expression studies. ImageJ was used to quantify the change in expression and compare the transcript profiles.

Western blot studies were executed to understand the differential protein expressions as per the previously mentioned protocol.[17,24] In brief, the complex of bDNA and peptides or Lipofectamine 2000 in DMEM without serum was treated to HCT-116 cells and incubated for around 4 h at 37°C in humidified conditions before the 1× PBS washing. Complete medium was added to each well and incubated for 48 h under the same conditions. Additionally, the radioimmunoprecipitation assay (RIPA) lysis buffer with protease inhibitor (NexGen HM Protease Inhibitor, Biopioneer, India) was used to generate the whole-cell lysate (WCL). The protein concentration was quantified using the Bradford reagent. Then 40 mg of protein were mixed with 2× Laemmli buffer and placed into a 10% SDS-PAGE (1:1). The PAGE was run for 2 h at 80 V, and protein bands were transferred onto the PVDF membranes. Then the PVDF membranes were blocked with 7.5% skim milk before being incubated with VEGF primary antibodies overnight at 4°C. Following a three-time wash every 5 min with 1× TBST, the membranes were incubated with the AP-conjugated secondary antibodies for 2 h under shaking conditions. The membrane was washed with 1× TBST three times to remove unbound secondary antibodies. Further, the blots were developed using 5 mL of AP buffer along with 16 μL of BCIP and 32 μL of NBT. The ImageJ software was used to analyze the western blot images while normalizing them to the GAPDH loading control.

Statistical analysis

All data are mean ± standard deviation with n = 3 or 5. The significance level was analyzed by one-way ANOVA, followed by Duncan's new multiple-range test. The statistical value of $p < 0.05$ was considered significant.

DATA AND CODE AVAILABILITY

The authors confirm that the data supporting the findings of this study are available within the article and its supplemental information.

SUPPLEMENTAL INFORMATION

Supplemental information can be found online at https://doi.org/10.1016/j.omtn.2023.07.017.

ACKNOWLEDGMENTS

This work was supported by the CSIR-Young Scientist Project (YSP-05) and Har Gobind Khorana DBT-Innovative Young Biotechnologist Fellow project (GAP-312) to U.S. The authors thankfully acknowledge the financial support by the DBT (grant no. BT/PR10019/NNT/28/708/2013) and DAE (grant no. 37(2)/14/22/2015/BRNS/37172), Government of India, to D.M. B.P. acknowledges the financial support from DBT-BIRAC (grant no BIRAC/KIIT0552/BIG14/19) and Startup Odisha (IEDO/BBSR/STARTUP-70/MBOSP-VOL-V/12/2021-22). Further, the authors are thankful to Dr. Amol Ratnakar Suryawanshi and Mr. R. Rajendra Kumar Reddy, Proteomic Facility, Institute of Life Sciences, Bhubaneswar, for assisting in MALDI-TOF analysis. The authors thank Dr. H.S. Biswal of the National Institute of Science Education and Research (NISER) for help in carrying out Isothermal titration calorimetry (ITC) studies in their laboratory. B.B. is thankful to Departmental of Science and Technology, Government of India, for the award of the INSPIRE Fellowship.

AUTHOR CONTRIBUTIONS

U.S. and D.M. initiated the project and designed the experiments. B.P. and B.B. carried out experiments and analyzed the data. K.D.T. performed the ITC. A.K. performed the RT-PCR. U.D. performed the microscopy. All the authors co-wrote the paper and commented on the manuscript. All authors have given approval for the submission of the manuscript.

DECLARATION OF INTERESTS

The authors declare no competing interests.

REFERENCES

1. Saminathan, A., Zajac, M., Anees, P., and Krishnan, Y. (2022). Organelle-level precision with next-generation targeting technologies. Nat. Rev. Mater. *7*, 355–371.
2. Hahn, J., Wickham, S.F.J., Shih, W.M., and Perrault, S.D. (2014). Addressing the instability of DNA nanostructures in tissue culture. ACS Nano *8*, 8765–8775.
3. Rajwar, A., Shetty, S.R., Vaswani, P., Morya, V., Barai, A., Sen, S., Sonawane, M., and Bhatia, D. (2022). Geometry of a DNA nanostructure influences its endocytosis: Cellular study on 2D, 3D, and in vivo systems. ACS Nano *16*, 10496–10508.
4. Jiang, S., Ge, Z., Mou, S., Yan, H., and Fan, C. (2021). Designer DNA nanostructures for therapeutics. Chem *7*, 1156–1179.
5. Dong, Y., Yao, C., Zhu, Y., Yang, L., Luo, D., and Yang, D. (2020). DNA functional materials assembled from branched DNA: Design, synthesis, and applications. Chem. Rev. *120*, 9420–9481.
6. Henry, S.J.W., and Stephanopoulos, N. (2021). Functionalizing DNA nanostructures for therapeutic applications. Wiley Interdiscip. Rev. Nanomed. Nanobiotechnol. *13*, e1729.
7. Shen, L., Wang, P., and Ke, Y. (2021). DNA nanotechnology-based biosensors and therapeutics. Adv. Healthc. Mater. *10*, e2002205.
8. Hu, Q., Wang, S., Wang, L., Gu, H., and Fan, C. (2018). DNA nanostructure-based systems for intelligent delivery of therapeutic oligonucleotides. Adv. Healthc. Mater. *7*, p1701153.
9. Baral, B., Nial, P.S., and Subudhi, U. (2023). Enhanced enzymatic activity and conformational stability of catalase in presence of tetrahedral DNA nanostructures: A biophysical and kinetic study. Int. J. Biol. Macromol. *242*, e124677.
10. Keller, A., and Linko, V. (2020). Challenges and perspectives of DNA nanostructures in biomedicine. Angew. Chem. Int. Ed. *59*, 15818–15833.
11. Huo, S., Li, H., Boersma, A.J., and Herrmann, A. (2019). DNA nanotechnology enters cell membranes. Adv. Sci. *6*, e1900043.
12. Hossen, M.N., Murphy, B., Garcı a-Hevia, L., Bhattacharya, R., and Mukherjee, P. (2018). Probing cellular processes using engineered nanoparticles. Bioconjugate Chem. *29*, 1793–1808.
13. Neuhaus, B., Tosun, B., Rotan, O., Frede, A., Westendorf, A.M., and Epple, M. (2016). Nanoparticles as transfection agents: A comprehensive study with ten different cell lines. RSC Adv. *6*, 18102–18112.
14. Chernousova, S., and Epple, M. (2017). Live-cell imaging to compare the transfection and gene silencing efficiency of calcium phosphate nanoparticles and a liposomal transfection agent. Gene Ther. *24*, 282–289.
15. Aliabadi, H.M., Landry, B., Bahadur, R.K., Neamnark, A., Suwantong, O., and Uludağ, H. (2011). Impact of lipid substitution on assembly and delivery of siRNA by cationic polymers. Macromol. Biosci. *11*, 662–672.

16. Salehi, D., Mozaffari, S., Zoghebi, K., Lohan, S., Mandal, D., Tiwari, R.K., and Parang, K. (2022). Amphiphilic cell-penetrating peptides containing natural and unnatural amino acids as drug delivery agents. Cells *11*, e1156.

17. Panigrahi, B., Mishra, S., Singh, R.K., Siddiqui, N., Bal, R., and Mandal, D. (2019). Peptide generated anisotropic gold nanoparticles as efficient siRNA vectors. Int. J. Pharm. *563*, 198–207.

18. Rana, S., Bhatnagar, A., Singh, S., and Prabhakar, N. (2022). Evaluation of liver specific ionizable lipid nanocarrier in the delivery of siRNA. Chem. Phys. Lipids *246*, e105207.

19. Morris, M.C., Vidal, P., Chaloin, L., Heitz, F., and Divita, G. (1997). A new peptide vector for efficient delivery of oligonucleotides into mammalian cells. Nucleic Acids Res. *25*, 2730–2736.

20. Montrose, K., Yang, Y., Sun, X., Wiles, S., and Krissansen, G.W. (2013). Xentry, a new class of cell-penetrating peptide uniquely equipped for delivery of drugs. Sci. Rep. *3*, e1661.

21. Coutinho, F.P., Green, C.R., and Rupenthal, I.D. (2018). Intracellular oligonucleotide delivery using the cell penetrating peptide Xentry. Sci. Rep. *8*, 11256–11310.

22. Mäe, M., and Langel, Ü. (2006). Cell-penetrating peptides as vectors for peptide, protein and oligonucleotide delivery. Curr. Opin. Pharmacol. *6*, 509–514.

23. Asseline, U., Gonçalves, C., Pichon, C., and Midoux, P. (2014). Improved nuclear delivery of antisense 2'-Ome RNA by conjugation with the histidine-rich peptide H5WYG. J. Gene Med. *16*, 157–165.

24. Panigrahi, B., Singh, R.K., Suryakant, U., Mishra, S., Potnis, A.A., Jena, A.B., Kerry, R.G., Rajaram, H., Ghosh, S.K., and Mandal, D. (2022). Cyclic peptides nanospheres: A '2-in-1' self-assembled delivery system for targeting nucleus and cytoplasm. Eur. J. Pharmaceut. Sci. *171*, e106125.

25. Shirazi, A.N., Mozaffari, S., Sherpa, R.T., Tiwari, R., and Parang, K. (2018). Efficient intracellular delivery of cell-impermeable cargo molecules by peptides containing tryptophan and histidine. Molecules *23*, p1536.

26. Mandal, D., Nasrolahi Shirazi, A., and Parang, K. (2011). Cell-penetrating homochiral cyclic peptides as nuclear-targeting molecular transporters. Angew. Chem. Int. Ed. *50*, 9633–9637.

27. Panigrahi, B., Singh, R.K., Mishra, S., and Mandal, D. (2018). Cyclic peptide-based nanostructures as efficient siRNA carriers. Artif. Cells, Nanomed. Biotechnol. *46*, 763–773.

28. Neufeld, G., Cohen, T., Gengrinovitch, S., and Poltorak, Z. (1999). Vascular endothelial growth factor (VEGF) and its receptors. FASEB. J. *13*, 9–22.

29. Eichmann, A., and Simons, M. (2012). VEGF signaling inside vascular endothelial cells and beyond. Curr. Opin. Cell Biol. *24*, 188–193.

30. McMahon, G. (2000). VEGF receptor signaling in tumor angiogenesis. Oncol. *5*, 3–10.

31. Saharinen, P., Eklund, L., Pulkki, K., Bono, P., and Alitalo, K. (2011). VEGF and angiopoietin signaling in tumor angiogenesis and metastasis. Trends Mol. Med. *17*, 347–362.

32. Paauwe, M., Heijkants, R.C., Oudt, C.H., Van Pelt, G.W., Cui, C., Theuer, C.P., Hardwick, J.C.H., Sier, C.F.M., and Hawinkels, L.J.A.C. (2016). Endoglin targeting inhibits tumor angiogenesis and metastatic spread in breast cancer. Oncogene *35*, 4069–4079.

33. Nayak, A.K., and Subudhi, U. (2014). Directed self-assembly of genomic sequences into monomeric and polymeric branched DNA structures. RSC Adv. *4*, 54506–54511.

34. Kar, A., Kumari, K., Mishra, S.K., and Subudhi, U. (2022). Self-assembled DNA nanostructure containing oncogenic miRNA-mediated cell proliferation by downregulation of FOXO1 expression. BMC Cancer *22*, 1332–1410.

35. Nahar, S., Nayak, A.K., Ghosh, A., Subudhi, U., and Maiti, S. (2018). Enhanced and synergistic downregulation of oncogenic miRNAs by self-assembled branched DNA. Nanoscale *10*, 195–202.

36. Nayak, A.K., Rath, S.K., and Subudhi, U. (2019). Preparation of stable branched DNA nanostructures: Process of cooperative self-assembly. J. Phys. Chem. B *123*, 3591–3597.

37. Di Antonio, M., Ponjavic, A., Radzevičius, A., Ranasinghe, R.T., Catalano, M., Zhang, X., Shen, J., Needham, L.M., Lee, S.F., Klenerman, D., and Balasubramanian, S. (2020). Single-molecule visualization of DNA G-quadruplex formation in live cells. Nat. Chem. *12*, 832–837.

38. Woody, R.W. (1985). Circular dichroism of peptides. Conformation in Biology and Drug Design (Academic Press), pp. 15–114.

39. Migliore, M., Bonvicini, A., Tognetti, V., Guilhaudis, L., Baaden, M., Oulyadi, H., Joubert, L., and Ségalas-Milazzo, I. (2020). Characterization of β-turns by electronic circular dichroism spectroscopy: A coupled molecular dynamics and time-dependent density functional theory computational study. Phys. Chem. Chem. Phys. *22*, 1611–1623.

40. Rosenbaum, D.M., Rasmussen, S.G.F., and Kobilka, B.K. (2009). The structure and function of G-protein-coupled receptors. Nature *459*, 356–363.

41. Foster, S.R., Hauser, A.S., Vedel, L., Strachan, R.T., Huang, X.P., Gavin, A.C., Shah, S.D., Nayak, A.P., Haugaard-Kedström, L.M., Penn, R.B., et al. (2019). Discovery of human signaling systems: Pairing peptides to G-protein-coupled receptors. Cell *179*, 895–908.

42. Tyndall, J.D.A., Pfeiffer, B., Abbenante, G., and Fairlie, D.P. (2005). Over one hundred peptide-activated G-protein-coupled receptors recognize ligands with turn structure. Chem. Rev. *105*, 793–826.

43. Lehninger, A.L., Nelson, D.L., David, L., and Cox, M.M. (2005). Lehninger principles of biochemistry Macmillan, 5 Edn, pp. 1–1119.

44. Kim, G.C., Cheon, D.H., and Lee, Y. (2021). Challenge to overcome current limitations of cell-penetrating peptides. Biochim. Biophys. Acta, Proteins Proteomics *1869*, e140604.

45. Tuttolomondo, M., Casella, C., Hansen, P.L., Polo, E., Herda, L.M., Dawson, K.A., Ditzel, H.J., and Mollenhauer, J. (2017). Human DMBT1-Derived Cell-Penetrating Peptides for Intracellular siRNA Delivery. Mol. Ther. Nucleic Acids *8*, 264–276.

46. Kim, D., Kim, V., McCarty, K.D., and Guengerich, F.P. (2021). Tight binding of cytochrome b5 to cytochrome P450 17A1 is a critical feature of stimulation of C21 steroid lyase activity and androgen synthesis. J. Biol. Chem. *296*, e100571.

47. Ishida, T., Tarui, M., In, Y., Ogiyama, M., Doi, M., and Inoue, M. (1993). Cooperative face-to-face and edge-to-face aromatic interactions of tryptophan indole ring with N7-quarternized guanine and neutral cytosine bases. FEBS Lett. *333*, 214–216.

48. Calladine, C.R., Drew, H.R., Luisi, B.F., and Travers, A.A. (2004). Understanding DNA: The Molecule and How it Works (Elsevier *3rd*), pp. 1–334.

49. Ross, P.D., and Subramanian, S. (1981). Thermodynamics of protein association reactions: forces contributing to stability. Biochemistry *20*, 3096–3102.

50. Zhang, C., Ko, S.H., Su, M., Leng, Y., Ribbe, A.E., Jiang, W., and Mao, C. (2009). Symmetry controls the face geometry of DNA polyhedra. J. Am. Chem. Soc. *131*, 1413–1415.

51. Watson, J.D., and Crick, F.H.C. (1953). Molecular structure of nucleic acids: A structure for deoxyribose nucleic acid. Nature *171*, 737–738.

52. Baral, B., Dutta, J., and Subudhi, U. (2021). Biophysical interaction between self-assembled branched DNA nanostructures with bovine serum albumin and bovine liver catalase. Int. J. Biol. Macromol. *177*, 119–128.

53. Gershon, H., Ghirlando, R., Guttman, S.B., and Minsky, A. (1993). Mode of formation and structural features of DNA-cationic liposome complexes used for transfection. Biochemistry *32*, 7143–7151.

54. Templeton, N.S., Lasic, D.D., Frederik, P.M., Strey, H.H., Roberts, D.D., and Pavlakis, G.N. (1997). Improved DNA:liposome complexes for increased systemic delivery and gene expression. Nat. Biotechnol. *15*, 647–652.

55. Nayak, A.K., Mishra, A., Jena, B.S., Mishra, B.K., and Subudhi, U. (2016). Lanthanum induced B-to-Z transition in self-assembled Y-shaped branched DNA structure. Sci. Rep. *6*, e26855.

56. Wamhoff, E.C., Romanov, A., Huang, H., Read, B.J., Ginsburg, E., Knappe, G.A., Kim, H.M., Farrell, N.P., Irvine, D.J., and Bathe, M. (2022). Controlling Nuclease Degradation of Wireframe DNA Origami with Minor Groove Binders. ACS Nano *16*, 8954–8966.

57. Cherepanova, A., Tamkovich, S., Pyshnyi, D., Kharkova, M., Vlassov, V., and Laktionov, P. (2007). Immunochemical assay for deoxyribonuclease activity in body fluids. J. Immunol. Methods *325*, 96–103.

58. Mótyán, J.A., Tóth, F., and Tőzsér, J. (2013). Research Applications of Proteolytic Enzymes in Molecular Biology. Biomolecules *3*, 923–942.

59. White, L.J., Taylor, A.J., Faulk, D.M., Keane, T.J., Saldin, L.T., Reing, J.E., Swinehart, I.T., Turner, N.J., Ratner, B.D., and Badylak, S.F. (2017). The impact of detergents on the tissue decellularization process: A ToF-SIMS study. Acta Biomater. *50*, 207–219.

60. Shcheynikov, N., Son, A., Hong, J.H., Yamazaki, O., Ohana, E., Kurtz, I., Shin, D.M., and Muallem, S. (2015). Intracellular Cl^- as a signaling ion that potently regulates Na^+/HCO^{3-} Transporters. Proc. Natl. Acad. Sci. USA *112*, E329–E337.

61. Takemoto, H., Ishii, A., Miyata, K., Nakanishi, M., Oba, M., Ishii, T., Yamasaki, Y., Nishiyama, N., and Kataoka, K. (2010). Polyion complex stability and gene silencing efficiency with a siRNA-grafted polymer delivery system. Biomaterials *31*, 8097–8105.

62. Son, K.K., Patel, D.H., Tkach, D., and Park, A. (2000). Cationic liposome and plasmid DNA complexes formed in serum-free medium under optimum transfection condition are negatively charged. Biochim. Biophys. Acta *1466*, 11–15.

63. Young, D.S. (1997). Effects of drugs on clinical laboratory tests. Ann. Clin. Biochem. *34*, 579–581.